

Optical-phonon states of SiC small particles studied by Raman scattering and infrared absorption

Y. Sasaki* and Y. Nishina

Institute for Materials Research, Tohoku University, Sendai 980, Japan

M. Sato[†] and K. Okamura[‡]

The Oarai Branch, Institute for Materials Research, Tohoku University, Oarai, Ibaraki 311-13, Japan

(Received 18 January 1989)

The particle-size dependence of frequencies and dampings of optical phonons is studied from analyses of Raman-scattering and infrared-absorption spectra of SiC small particles. The particle size ranges from a few nanometers to more than 1 μm . The measured spectra are explained qualitatively in terms of a model of a core plasmon and a carrier-free layer on the surface (shell) of the particles, provided that their sizes are larger than about 30 nm. Here we use Mie's scattering equation or the averaged dielectric function of Maxwell-Garnet. The thickness of the shell is 5–40 nm depending on the sample. If the particle size is smaller than about 200 nm, phonon parameters, such as the TO-phonon frequency (ω_T), the LO-phonon frequency (ω_L) and their dampings, depend on the particle size rather than on the size of the crystallites which constitute the particle. For smaller particles, both ω_T and $\omega_L - \omega_T$ become smaller and the damping of the phonon becomes larger. The decrease in ω_T and increase in the phonon damping are correlated with the lattice imperfection near the surface. The decrease in $\omega_L - \omega_T$ is related to the absence of a contribution to the macroscopic electric field from the hypothetical atoms outside the particle and to the existence of the surface layer which gives little contribution to the macroscopic field. For particle sizes of a few nanometers, the absorption spectrum exhibits a combination of a crystal-like component and a broad symmetric line as expected for amorphous materials. The origin of the latter is attributed to the "surface layer," which is about 1 nm thick with lattice imperfection.

I. INTRODUCTION

The confinement of an elementary excitation in a small volume exhibits various kinds of electronic effects not observable in bulk materials. The electronic energy levels become discrete upon the confinement, and the energy band gap increases.^{1–3} The infrared-absorption spectrum and Raman spectrum of infrared-active phonons are dominated by the surface polariton (SP) rather than the bulk-mode polariton if the particle size is much smaller than the wavelength of light.^{4–6} These effects are explained in terms of confinement of an elementary excitation into the particle.

For particles smaller than a few tens of nanometers, the role of surface atoms becomes important. For example, the size dependence of the Debye temperature and of the melting point for small (< 100 nm) metallic particles have been explained in terms of softening of the lattice vibration for a surface layer with a thickness of 1–2 atomic layer(s).^{7–11} If the number of surface atoms of a particle is comparable to that of the inner atoms, the phonon in the particle is expected to be quite different from that in bulk crystals. The critical size, if it exists, is expected to be about 3 nm for a lattice constant of 0.3 nm. For small particles of Si and Ge, the Raman spectrum is "amorphouslike" if the particle size is smaller than about 10 nm, while a "crystal-like" spectrum is observed if the size is larger than 10 nm.^{12–15} The Raman spectrum of small

particles of PbI_2 shows sharp lines even if its size is as small as 2 nm.¹⁶ The TO and LO phonons, however, are highly damped for particles aggregated from acetone colloidal suspension.¹⁶ Thus a general rule has not been established for the size where the crystalline phonon model breaks down.

The purpose of this paper is to examine the size dependence of the phonon state in polar semiconductors as the size decreases from a few micrometers to a few nanometers. The phonon frequencies and damping are deduced from Raman spectra and infrared-absorption spectra. SiC is a suitable material for the present subject, because its optical-phonon frequencies are very high (796 and 972 cm^{-1}) so that the frequency shift of the phonon can be large enough to be detected even for a small fractional change in the phonon state. A preliminary study of our SiC particles made from polycarbosilane indicates that the plasmon is overdamped and a depression layer covers the surface of those particles.¹⁷

In Sec. II we explain the theoretical background of the absorption and Raman spectra of small particles in the frameworks of Maxwell-Garnett¹⁸ (MG) and Mie.¹⁹ Both approximations are based on the electromagnetic equation without or with the retardation effect, respectively. The experimental procedure is explained in Sec. III and the experimental result is presented in Sec. IV. In Sec. V we discuss the mechanism of the variation in the phonon frequency, the damping, and the LO-phonon-TO-

phonon splitting ($\omega_L - \omega_T$) of the optical phonon with respect to the particle size from 30 to 300 nm. The particle size where the crystalline approach breaks down is estimated for SiC. In explaining the experimental results we assume that the particle is a sphere and that it consists of a core with free carriers and a shell without carriers. Furthermore, we introduce a "surface layer" (a few atomic layers thick) which contains imperfections in the atomic arrangement. Preliminary results of this work have been published elsewhere.²⁰

II. CALCULATION OF ABSORPTION AND RAMAN SPECTRA

A. Absorption spectra

We assume in the calculation of absorption and Raman spectra that particles are distributed uniformly in a host medium with the dielectric constant of ϵ_m . The dielectric constant of the particle in the shell is given by

$$\epsilon_s(\omega) = \epsilon_\infty \left[1 + \frac{\omega_L^2 - \omega_T^2}{\omega_T^2 - \omega^2 - i\omega\Gamma_s} \right], \quad (1)$$

and in the core by

$$\epsilon_c(\omega) = \epsilon_\infty \left[1 + \frac{\omega_L^2 - \omega_T^2}{\omega_T^2 - \omega^2 - i\omega\Gamma_c} - \frac{\omega_p^2}{\omega^2 + i\omega\gamma} \right], \quad (2)$$

where ϵ_∞ is the high-frequency dielectric constant, ω_T (ω_L) is TO- (LO-) phonon frequency, Γ_s and Γ_c are damping constants of the optical phonon in the shell and core, respectively, γ is the damping of the plasmon in the core, and $\omega_p = (4\pi n e^2 / m^* \epsilon_\infty)^{1/2}$ is the plasma frequency, where n and m^* are carrier density and effective mass of the free carrier.

In the MG, or nonretarded, approximation the average

$$\begin{aligned} a_{l,1} = & \{ \epsilon_c [k_2 r_c j_l(k_2 r_c)]' j_l(k_1 r_c) - \epsilon_s j_l(k_2 r_c) [k_1 a_j l(k_1 r_c)]' \} \\ & \times \{ \epsilon_m [k_2 r_s n_l(k_2 r_s)]' j_l(k_1 r_s) - \epsilon_s n_l(k_2 r_s) [k_3 r_s j_l(k_3 r_s)]' \} \\ & - \{ \epsilon_c [k_2 r_c n_l(k_2 r_c)]' j_l(k_2 r_c) - \epsilon_s n_l(k_2 r_c) [k_1 r_c j_l(k_1 r_c)]' \} \\ & \times \{ \epsilon_m [k_2 r_s j_l(k_2 r_s)]' j_l(k_3 r_s) - \epsilon_s j_l(k_2 r_s) [k_3 r_s j_l(k_3 r_s)]' \}, \end{aligned} \quad (10)$$

$$\begin{aligned} b_{l,1} = & \epsilon_c \{ [k_2 r_c j_l(k_2 r_c)]' j_l(k_1 r_c) - j_l(k_2 r_c) [k_1 r_c j_l(k_1 r_c)]' \} \\ & \times \epsilon_s \{ [k_2 r_s n_l(k_2 r_s)]' j_l(k_3 r_s) - n_l(k_2 r_s) [k_3 r_s j_l(k_3 r_s)]' \} \\ & - \epsilon_c \{ [k_2 r_c n_l(k_2 r_c)]' j_l(k_1 r_c) - n_l(k_2 r_c) [k_1 r_c j_l(k_1 r_c)]' \} \\ & \times \epsilon_s \{ [k_2 r_s j_l(k_2 r_s)]' j_l(k_3 r_s) - j_l(k_2 r_s) [k_3 r_s j_l(k_3 r_s)]' \}. \end{aligned} \quad (11)$$

Here, j_l and n_l are the l th spherical Bessel and Neumann functions, respectively, the primes denote differentiation with respect to their arguments, and $k_1 = (\epsilon_c)^{1/2} \omega / c$, $k_2 = (\epsilon_s)^{1/2} \omega / c$, and $k_3 = (\epsilon_m)^{1/2} \omega / c$. $a_{l,2}$ and $b_{l,2}$ are obtained by replacing $j_l(k_3 r_s)$ with $h_l(k_3 r_s)$ in Eqs. (10) and (11), where h_l denotes a spherical Hankel function. The total cross section of the sphere including the absorption and scattering terms is given in units of its geometrical

dielectric constant $\epsilon_{av}(\omega)$ of the dielectric sphere-medium composite is given by²¹

$$\epsilon_{av}(\omega) = \frac{f \epsilon_c A_c R_{c-s}^3 + f \epsilon_s A_s (1 - R_{c-s}^3) + \epsilon_m}{f A_c R_{c-s}^3 + f A_s (1 - R_{c-s}^3) + 1 - f}, \quad (3)$$

where

$$A_c = 3\epsilon_s B, \quad (4)$$

$$A_s = (\epsilon_c + 2\epsilon_s) B, \quad (5)$$

and

$$B = \frac{3\epsilon_m}{(\epsilon_s + 2\epsilon_m)(2\epsilon_s + \epsilon_c) - 2(\epsilon_s - \epsilon_m)(\epsilon_s - \epsilon_c)R_{c-s}^3}. \quad (6)$$

Here, f is the volume-filling factor of spheres, and $R_{c-s} = r_c / r_s$ is the ratio of the radius of core, r_c , with respect to the radius of the sphere r_s . This approximation is not valid for large spheres because the retardation effect is not taken into account. The absorption coefficient of the composite can be calculated with $\epsilon_{av}(\omega)$ by

$$\alpha(\omega) = \frac{\omega \text{Im}[\epsilon_{av}(\omega)]}{c \text{Re}[(\epsilon_{av}(\omega))^{1/2}]}. \quad (7)$$

The total extinction cross section of a dielectric sphere with retardation is calculated with the generalized Mie coefficient²²

$$a_l = a_{l,1} / a_{l,2}, \quad (8)$$

$$b_l = b_{l,1} / b_{l,2}, \quad (9)$$

where

cross section by

$$\sigma(\omega) = \frac{2}{(k_3 r_s)^2} \sum_{l=1}^{\infty} (2l+1) \text{Re}(a_l + b_l). \quad (12)$$

The extinction coefficient $K(\omega)$ is given by

$$K(\omega) = \frac{3f\sigma(\omega)}{4r_s}, \quad (13)$$

for a system with small f , where the multiple scattering of the light is negligible. Identical line shapes are obtained by the calculations from the approach of MG and from Mie's, if the particle size is small enough ($r_s < 100$ nm for SiC) and if f is small.

Figure 1 shows the SP frequencies of a SiC sphere with free carriers covered by a carrier-free shell plotted as a function of ω_p for $\Gamma_c = \Gamma_s = 1 \text{ cm}^{-1}$ and $\gamma = 5 \text{ cm}^{-1}$ with Mie's formula. Branches noted as SL_- and SL_+ are SP's of the LO-phonon-plasmon coupled mode in the core, and S is the SP localized in the shell. In the limit of $\omega_p = 0$, SL_- and SL_+ approach 0 and ω_L , respectively, and S approaches the Fröhlich frequency ω_F defined by $\epsilon(\omega_F) = -2\epsilon_m$. The S branch approaches ω_L in the limit of $\omega_p \rightarrow \infty$.

An example of the spectrum of the extinction cross section $\sigma(\omega)$, is shown in Fig. 2. The SL_- and SL_+ lines are much weaker than the S line for ω_p smaller than ω_T , while the SL_+ line becomes dominant if $\omega_p \gg \omega_T$. The SL_+ line has intensity comparable to S if $\omega_p \approx \omega_L$. The relative intensity of the S line with respect to SL_+ increases with the ratio $(r_s - r_c)/r_s$. The absorption line due to the bulk polariton is much weaker than that caused by SP if $r < 100$ nm. Following the MG formula, the S mode splits into two for a finite value of f and the splitting increases with f . The lower-lying branch (S_T) is connected with the TO phonon and the other (S_L) with the LO phonon for $f \rightarrow 1$.

The extinction (and absorption) spectrum is modified considerably if $\gamma > \omega_p$ (overdamped plasmon) as shown in Fig. 3. The peak due to SL_+ shifts to lower frequency and its linewidth increases with increase in γ . For $\gamma > 1000 \text{ cm}^{-1}$, a dip is observed near ω_L .

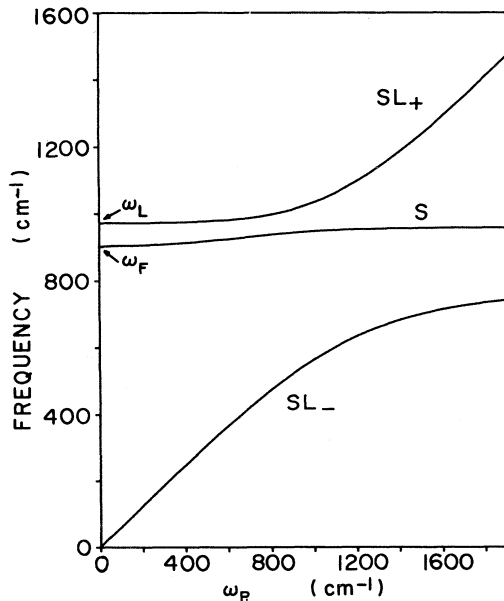


FIG. 1. Surface-polariton frequencies plotted as a function of ω_p for a SiC sphere consisting of the core with free carriers and the shell without carriers. Here, $r_s = 100$ nm, $r_c = 90$ nm, $\Gamma_c = \Gamma_s = 1 \text{ cm}^{-1}$, and $\gamma = 5 \text{ cm}^{-1}$.

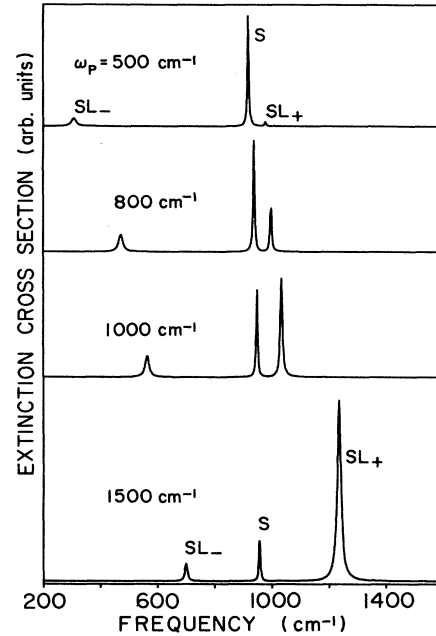


FIG. 2. Extinction spectra of a SiC sphere with the core-shell structure for several plasmon frequencies with $r_s = 100$ nm, $r_c = 90$ nm, $\Gamma_c = \Gamma_s = 1 \text{ cm}^{-1}$, and $\gamma = 10 \text{ cm}^{-1}$.

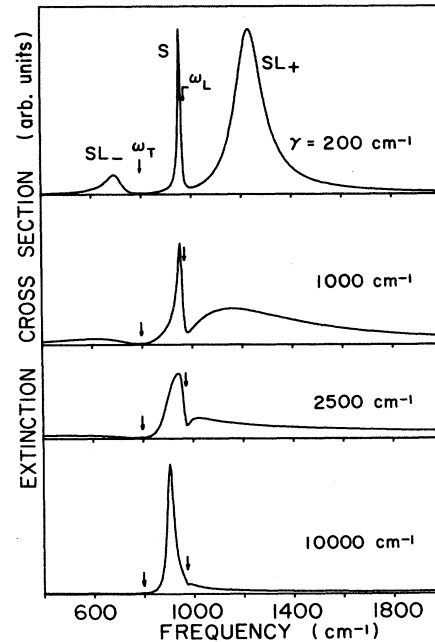


FIG. 3. Extinction spectra of a SiC particle with the core-shell structure calculated for several values of plasmon damping γ . Here, $r_s = 100$ nm, $r_c = 90$ nm, $\Gamma_c = \Gamma_s = 1 \text{ cm}^{-1}$, and $\omega_p = 1500 \text{ cm}^{-1}$.

B. Raman spectra

We calculate the Raman spectrum of the SP in small particles in the MG approach. The Faust-Henry coefficient, denoted by C_{FH} , is modified in the framework of the MG theory to²³

$$C_{\text{FH av}} = C_{\text{FH}} \left[\frac{\epsilon_{\infty \text{ av}} \omega_T^2 (\omega_{L \text{ av}}^2 - \omega_{T \text{ av}}^2)}{f \epsilon_{\infty} \omega_{T \text{ av}}^2 (\omega_L^2 - \omega_T^2)} \right]^{1/2}, \quad (14)$$

where $\epsilon_{\infty \text{ av}}$, $\omega_{T \text{ av}}$, and $\omega_{L \text{ av}}$ are the high-frequency dielectric constant, TO-phonon frequency, and LO-phonon frequency of the sphere-medium composite, respectively. These values are estimated from Eq. (3) with $\omega_p = \Gamma_s = \Gamma_c = 0$: $\epsilon_{\infty \text{ av}}$ is obtained in the limit of $\omega \rightarrow \infty$, $\omega_{T \text{ av}}$ is deduced by letting the denominator be zero, and $\omega_{L \text{ av}}$ is calculated from $\epsilon_{\text{av}}(\omega_{L \text{ av}}) = 0$. Here the Faust-Henry coefficient characterizes the ω dependence of the ratio of contributions from the electro-optic and deformation-potential terms to the Raman cross section. The Raman cross section is calculated with a formula which is valid even for large phonon and plasmon damping.^{24–26} The k dependence of the dielectric constant is negligible in the present case, where $m^* \approx 0.3m_0$, $n < 10^{20} \text{ cm}^{-3}$, $\omega_T \approx 800 \text{ cm}^{-1}$, and $\epsilon_{\infty} = 6.70$. The charge-fluctuation term is dropped because it is known to be very small compared to the deformation-potential and electro-optic terms.²⁷ The Raman spectrum due to SP is calculated by

$$I_R = D \Delta(Q, k) f^2 \omega_s^4 \left[\frac{d\alpha}{dE} \right] [n_q(\omega) + 1] \times \{ C_T \text{Im}[\epsilon_{\text{av}}(\omega)] + \text{Im}[-C_L(\omega)/\epsilon_{\text{av}}(\omega)] \}, \quad (15)$$

where the first term in the curly brackets gives the contribution from the transverse component and the second from the longitudinal. D is a constant, and $n_q(\omega)$ is the Bose factor. As explained later, $\Delta(Q, k)$ appears instead of the δ function for the momentum conservation in the Raman-scattering process. This term reflects the relaxation of the momentum-conservation rule due to the finite scattering volume of a small particle. C_T and C_L are given by²⁴

$$C_T = \left[\frac{C_{\text{FH av}} \omega_T^2}{\epsilon_{\infty \text{ av}} (\omega_L^2 - \omega_T^2)} \right]^2 \quad (16)$$

and

$$C_L(\omega) = 1 + 2C_{\text{FH av}} L_{\text{av}}(\omega) - \frac{C_{\text{FH av}}^2 \omega_{T \text{ av}}^2}{\omega_{L \text{ av}}^2 - \omega_{T \text{ av}}^2} \left[1 - \frac{\omega_{p \text{ av}}^2}{\omega^2 + i\omega\gamma} \right] L_{\text{av}}(\omega), \quad (17)$$

where

$$L_{\text{av}}(\omega) = \omega_{T \text{ av}}^2 / (\omega_{T \text{ av}}^2 - \omega^2 - i\omega\Gamma_{\text{av}}). \quad (18)$$

We take $\Gamma_{\text{av}} = \Gamma_c$ in the evaluation of Eq. (18). $\omega_{p \text{ av}}$ is calculated by⁵

$$\omega_{p \text{ av}} = \omega_p \left[\frac{\epsilon_{\infty} (1 + 2f)}{\epsilon_{\infty} (1 + 2f) + 2\epsilon_m (1 - f)} R_{c-s}^3 \right]^{1/2}, \quad (19)$$

where the uniform distribution of the free carriers is assumed for simplicity. Since L_{av} and $\omega_{p \text{ av}}$ are used only for evaluation of C_L , the effect of these simplifications is expected to be small.

$\Delta(Q, k)$ is written as⁶

$$\Delta(Q, k) = \frac{1}{\pi} \frac{k_i + 1/r_s}{(Q - k_r)^2 + (k_i + 1/r_s)^2}, \quad (20)$$

where Q is the change in the momentum of light in the scattering process and $k = k_r + ik_i$ is the complex radial wave vector of the polariton. $Q \approx 5 \times 10^5 \text{ cm}^{-1}$ in the backscattering configuration and Q can be as small as 10^3 cm^{-1} in forward scattering. For SP in a SiC particle of $r_s < 100 \text{ nm}$, it is estimated that $1/r_s \gg k_i$, k_r , and $k_r < 2 \times 10^4 \text{ cm}^{-1}$. Thus Eq. (20) is reduced to

$$\Delta(Q, k) \approx \frac{1}{\pi} \frac{1/r_s}{(Q - k_r)^2 + 1/r_s^2}. \quad (21)$$

We find from Eq. (21) that the Raman intensity of a SP is stronger in the forward-scattering geometry than in backscattering, similar to the case of a SP in a slab.²⁸

For the bulk mode, the Raman spectrum is calculated for the core and shell separately from

$$I_R = DV_r \Delta(Q, k) f \omega_s^4 \left[\frac{d\alpha}{dE} \right] [n_q(\omega) + 1] \times \{ C_T \text{Im}[\epsilon_{c,s}(\omega)] + \text{Im}[-C_L(\omega)/\epsilon_{c,s}(\omega)] \}, \quad (22)$$

where the volume factor V_r is equal to R_{c-s}^3 for the core and to $1 - R_{c-s}^3$ for the shell. In the calculation of C_T and C_L we replace $C_{\text{FH av}}$, $\omega_{T \text{ av}}$, $\omega_{L \text{ av}}$, $\omega_{p \text{ av}}$, and $\epsilon_{\infty \text{ av}}$ in Eqs. (16) and (17) by the values for bulk SiC. In the evaluation of $\Delta(Q, k)$, k_r is determined from the boundary condition that the radial part of the wave function is assumed to be zero at the surface of the sphere.⁶ We obtain $k_r = l\pi/2r_s$ for the l th mode. Finally, we take a summation of contributions from the SP, the bulk polariton in the core, and that in the shell.

A minimum exists in the value of k_r of the bulk polariton as determined by the boundary condition. For example, $k_r \geq 5 \times 10^5 \text{ cm}^{-1}$ if $r_s = 50 \text{ nm}$, while Q may be changed from 10^3 to 10^5 cm^{-1} depending on the scattering angle. If we apply these conditions to Eq. (20), we find that the Raman intensity of the bulk mode in small particles is weaker in the forward-scattering geometry than in backscattering, in contrast to the case of a SP. Multiple scattering of the light by the particles makes the detection of the light scattered in the forward direction possible even in the backscattering configuration. Consequently, we underestimate the size of particles in the analysis of Raman spectra measured in the backscattering geometry if we use Eq. (20) and neglect the multiple-scattering effect.

III. EXPERIMENT

We have used two types of samples: one is made from polycarbosilane through a pyrolysis process in inert gas²⁹ and the other obtained from Ibigawa Electric Industries Co., Ltd. The latter has been produced through reaction

between silica and carbon. Its nominal size is about 120 nm as deduced by the surface-area method. The characterization of those SiC samples made from polycarbosilane shows that they consist of SiC small particles (either amorphous $\text{Si}_1\text{C}_{1+\delta}$ or microcrystalline SiC), carbon microcrystals, and silicon oxide if they are heat treated between about 800 and 1400 °C.³⁰ The SiC crystalline particle grows from the amorphous $\text{Si}_1\text{C}_{1+\delta}$ particle by heat treatment. All of the $\text{Si}_1\text{C}_{1+\delta}$ particles are turned to microcrystalline SiC if the heat-treatment temperature (HTT) is higher than about 1300 °C. If HTT exceeds about 1500 °C the excess carbon and silicon oxide react to form CO and SiC, and then CO is released. That process enhances coalescence of the SiC particles and their size increases rapidly. Our SiC particles consist mostly of the 3C polytype with a small mixture of the 2H polytype. Note that the pyrolysis process of the polycarbosilane has been developed to produce strong SiC fibers.²⁹

Raman spectra are obtained with a double-grating monochromator and a photon-counting system. The light source is an Ar⁺-ion laser beam (488 nm, 20 mW) focused to 0.1×2.5 mm² by a cylindrical lens. Those fibers or powders described above are placed in the air as obtained. The Raman spectra at higher temperatures up to 800 K are measured with samples in the Ar gas. Infrared-absorption spectra are measured with a double-beam grating spectrometer in the frequency range from 400 to 4000 cm⁻¹. The fibers are pulverized in a mortar made from silicon nitride ceramics. Then they are mixed with KBr powder and pressed to form a pellet. The volume-filling factor f of SiC particles is about 0.001. The particle size of SiC is larger than the crystallite size constituting the particle because of coalescence.³⁰ The particle size (L_{EM}) is estimated from electron-microscope observation and the size of crystallite (L_{111}) from the width of the [111] line in the x-ray-diffraction spectrum.

IV. RESULTS

A. Infrared-absorption spectra

Infrared-absorption spectra of SiC particles embedded in KBr are shown in Fig. 4 for two samples with different particle sizes. The experimental spectra show a dip near ω_L as predicted in Sec. II A (Fig. 3). The dip becomes shallower for larger particles because the volume ratio of shell to core decreases in larger particles. On the other hand, the structure at around ω_T is enhanced in larger particles since it comes from the bulk polariton.

The experimental spectra are much broader than the calculated spectra of SP with parameters summarized in Table I. The calculated peak position is blue shifted compared with the experimental results. The calculated linewidth of SP increases by 10% or 20% if we take into account the distribution of the particle size as estimated from transmission-electron-microscope (TEM) observation. The result, however, is far from a good fit. We get a reasonable fit if we assume that aggregation of particles occurs in the fabrication process of the pellet. The effect of aggregation is taken into account by increasing f in the MG formula. The dashed-dotted line in Fig. 4(a) is

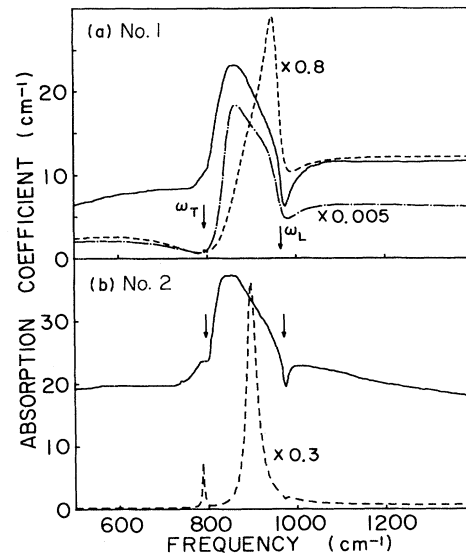


FIG. 4. Infrared-absorption spectra of SiC particles embedded in KBr. (a) shows the result for particles with $L_{EM} = 85 \pm 20$ nm, $f = 0.0013$, and (b) for those with L_{EM} ranging from 0.7 to 5 μm , $f = 0.002$. Solid lines represent experimental results, dashed lines show the calculated spectra with Mie's formula, and the dashed-dotted line in (a) gives a calculated absorption spectrum with the MG formula assuming $f = 0.65$. The parameters used in the calculations are summarized in Table I.

calculated with the MG formula [Eqs. (3)–(7)] assuming $f = 0.65$, instead of the experimental value of 0.0013. The peak position and width of the SP line fits quite well to the experimental result. The effect of aggregation has been studied for the optical-absorption spectra of small silver particles.³¹ The calculation of the absorption spectrum is rather complicated if we take into account both aggregation and retardation simultaneously. Thus we did not try the spectral calculation with aggregation for large particles, as in the case of Fig. 4(b) ($\approx 1 \mu\text{m}$).

Rieder, Ishigame, and Genzel³² report a dip near ω_L in the infrared-absorption spectra of small particles of CdO. They explain the anomaly in terms of the ω dependence of γ . Their spectrum, however, can be interpreted in terms of the presence of a depletion layer on the surface of the CdO particles with overdamped plasmon.

The absorption spectrum changes considerably if the particle size is smaller than a few nanometers. Figure 5 compares the absorption spectra of SiC made from polycarbosilane obtained after heat treatment at various temperatures. Spectrum (a) is measured for the sample of an HTT of 700 °C, which contains hydrogen.³³ The spectra of Figs. 5(b)–5(e) are measured for samples containing virtually no hydrogen. Small SiC particles up to 2 nm are observed by TEM for the sample exhibiting the absorption spectrum of Fig. 5(b). Each of those particles consists of a single crystal. The samples for Figs. 5(c)–5(e) consist of small SiC particles and silicon oxide. Here, $L_{EM} = 2 \pm 1$ nm and $L_{111} = 2$ nm for the sample of Fig. 5(c), $L_{EM} = 4 \pm 1$ nm and $L_{111} = 2.6$ nm for Fig. 5(d), and

TABLE I. Examples of fitting parameters for the infrared and Raman spectra of SiC small particles.

	Samples ^a				
	No. 1	No. 2	No. 3	No. 4	No. 5
ω_T (cm ⁻¹)	794	796	793	792	794
ω_L (cm ⁻¹)	965	972	969	958	962
Γ_c (cm ⁻¹)	5	2	10	17	12
Γ_s (cm ⁻¹)	25	5	35	30	35
ω_p (cm ⁻¹)	2500	750	3000	2500	2500
γ (cm ⁻¹)	4000	3300	5000	4000	4000
r_c/r_s	0.89	0.95	0.8	0.85	0.87
$2r_s$ (Raman, nm)	20	54	32	8	11
$2r_s$ (ir, nm)	240	1000	600	<200	<200
L_{111} (nm)	22	≥160	46	19	20
L_{EM} (nm) ^b	85±20	700-5000	140±80	30±8	38±9

^aSample no. 3 is made by Ibigawa Electric, Inc. and the others are made from polycarbosilane.

^bRange of the size distribution is deduced after curve fitting by a Gaussian, and denoted by mean value $\pm\sigma$.

$L_{EM}=30\pm 8$ nm and $L_{111}=19$ nm for Fig. 5(e). The absorption band around 1050 cm^{-1} comes from SiO stretching vibration.

Figure 5(e) shows a spectrum quite similar to that for the sample no. 1 [Fig. 4(a)]. Thus the spectrum of the SiC particles with their sizes down to 30 nm is explained in terms of small crystalline particles with modifications in the phonon parameters as discussed in the following section. A broad tail appears in the lower-frequency side

of the peak if the particle size is a few nanometers [Figs. 5(c) and 5(d)]. We find a change in the slope at a frequency slightly lower than 800 cm^{-1} , as shown by arrows. The absorption coefficient increases abruptly at around that frequency in Fig. 5(e). These features indicate that the absorption spectra of Figs. 5(c) and 5(d) are a superposition of the spectra for crystalline particles [Fig. 5(e)] and a broad band centered around 800 cm^{-1} . The absorption peak for the “crystal-like” component, however, seems to be red-shifted by a couple of tens of wave numbers. Although small SiC crystals up to 2 nm occupy a major part of the sample, the absorption spectrum of Fig. 5(b) does not show any of the features expected for crystalline particle. The spectrum is similar to the calculated density of phonon states with a large damping ($\approx 200\text{ cm}^{-1}$),^{30,34} which is expected for amorphous SiC; i.e., the spectrum is “amorphous-like.” The width of the SiC line is narrower with hydrogen [Fig. 5(a)] than that without hydrogen [Fig. 5(b)].

B. Raman spectra

Figure 6 shows the Raman spectra of SiC particles. Figure 6(a) is measured for porous SiC, where the volume-filling factor of SiC is expected to be high. The others are measured for powders which are placed on an adhesive tape. In these samples we let $\epsilon_m=1$. The line around ω_T comes from the bulk polariton and that around ω_L from bulk LO phonon with or without coupling to the plasmon. The components observed between ω_T and ω_L are due to the S-mode SP. The SL_+ and SL_- modes are damped because of large γ . The intensity of SP components is stronger with reference to the bulk modes in smaller particles. We find a sharp line and a broad band for the LO-phonon line in the spectrum of Fig. 6(c). The sharp component comes from the bare (uncoupled) LO phonon in the shell and the broad one from the coupled mode of the LO phonon and plasmon in the core. If the plasmon is overdamped the coupled LO-phonon line is very broad. The peak at ω_L comes from the bare LO phonon in the shell in Figs. 6(a) and 6(b).

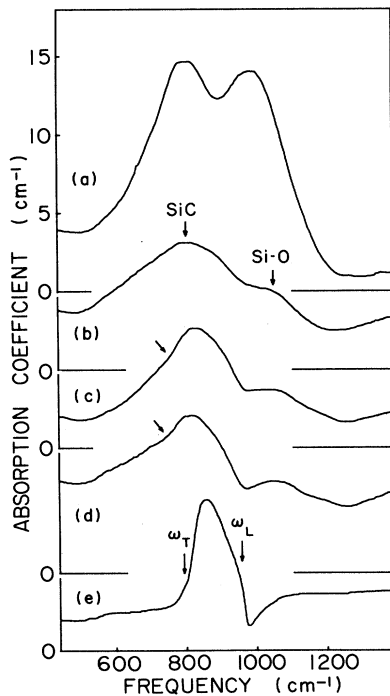


FIG. 5. Infrared-absorption spectra of SiC powdered and embedded in KBr. The absorption coefficient is reduced for $f=0.001$. (a) presents the result for the sample of a HTT of 700°C , (b) 1200°C , (c) 1300°C , (d) 1400°C , and (e) 1500°C . See text for particle and crystallite size.

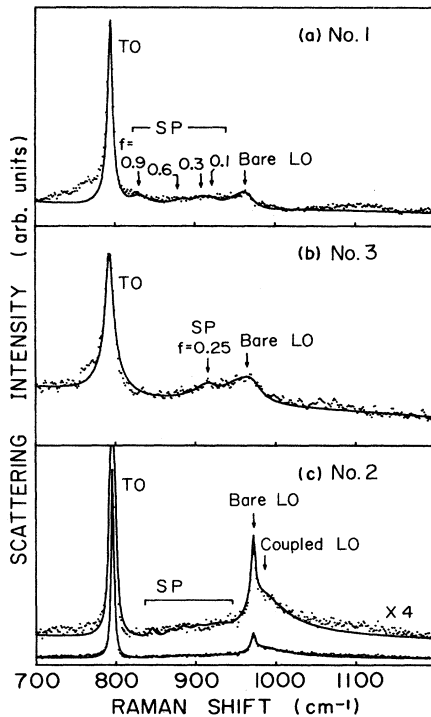


FIG. 6. Raman spectra of (a) porous SiC with $L_{EM}=85$ nm ($L_{111}=22$ nm), (b) SiC powders with $L_{EM}=140$ nm ($L_{111}=46$ nm), and (c) SiC powders with $L_{EM}=0.7\text{--}5$ μm ($L_{111}\geq 160$ nm). Dots show experimental results and solid lines present the calculated spectra. The arrows denote positions of the S_T -mode SP for a given filling factor f . The parameters used in the calculation are given in Table I.

The solid lines in Fig. 6 show the results of the curve fit, where we use $C_{FH}=0.21\pm 0.01$. A similar value of 0.25 is reported for the bulk crystal as estimated from the ratio of intensities of TO- and LO-phonon lines.²⁶ Our value, however, is smaller than the estimate based on the curve fit to the Raman line of the LO-phonon–plasmon coupled mode (0.35–0.39).^{26,27} Other parameters used for the fit are summarized in Table I. The carrier density is estimated to be about 2×10^{20} cm^{-3} for $\omega_p=3000$ cm^{-1} .

The curve fit shows that $f=0.25$ for the SiC powder of sample no. 3 [Fig. 6(b)]. This value of f is reasonable for lightly pressed small particles. It is necessary to assume a distribution of f ranging from 0.1 to 0.9 for the porous fiber corresponding to Fig. 6(a). Since the particle size of the sample for Fig. 6(c) is larger than the wavelength of the laser light, our curve fit with the MG formula does not give correct values for fitting parameters of r_s and f . The arrows in Figs. 6(a) and 6(b) indicate the positions of the S -mode SP with transverse character (S_T). The counterpart of SP with longitudinal character (S_L) stays near ω_L with a much wider linewidth than S_T . The disagreement between the calculation and experimental spectra below ω_T becomes larger in smaller particles. The existence of a rather broad line centered around 780 cm^{-1} has been found from a curve fit with Lorentzian

and Gaussian curves. This component has been ascribed to the amorphous part of the SiC fiber.³⁰

The frequencies of ω_T , $\omega_L - \omega_T$, and damping of the phonons in the core and shell are plotted in Fig. 7 as a function of $2r_s$, which is estimated from the curve fit to the Raman spectra. Both ω_T and $\omega_L - \omega_T$ decrease, especially the latter, with a decrease in r_s . The ω_L deduced here reflects the value in the shell, because the Raman line due to the LO phonon coupled with the plasmon in the core is extremely broad for the samples shown in Fig. 7 (and in Table I) with the exception of sample no. 2. The phonon damping increases with decrease in r_s . Γ_s increases more rapidly than Γ_c . The phonon parameters of sample no. 2 given in Table I agree with those of 3C-SiC crystal.³⁵

If the particle size is smaller than a few nanometers, the Raman spectrum does not show any sharp lines. A curve fit shows the existence of broad Raman bands corresponding to the phonon density of states of SiC,³⁰ i.e., the amorphouslike Raman spectrum is observed for particles smaller than a few nanometers. This result does not agree with that of the infrared absorption presented in Sec. IV A, where the crystal-like component is observed along with the amorphouslike component for particles with sizes of a few nanometers. The discrepancy may come from the following fact: We have measured the Raman spectra of the product as obtained. Its color

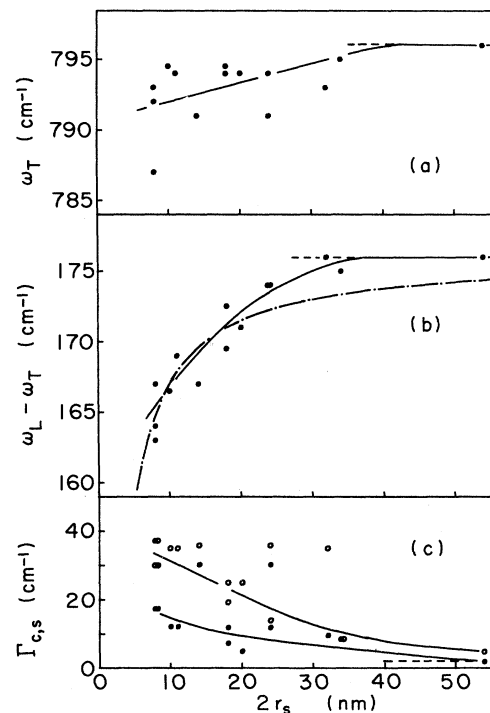


FIG. 7. (a) TO-phonon frequency, (b) $\omega_L - \omega_T$, and (c) phonon dampings as obtained by the curve fit and plotted as a function of $2r_s$. Open circles present Γ_s and solid circles show Γ_c , respectively, in (c). The values of r_s in this figure are estimated by the curves fit. Horizontal dashed lines give the values in the bulk crystals. The dashed-dotted line in (b) shows the calculated curve with $a_s=0.13$ nm.

with a HTT of $\leq 1400^\circ\text{C}$ (particle size less than a few nanometers) is black due to excess carbon. Then the Raman spectrum reflects the structure near the surface. On the other hand, the whole fiber is examined in the infrared spectroscopy. Thus the difference in the Raman and infrared spectra is attributed to the spatial distribution of the particle size. For samples with a HTT of $\geq 1500^\circ\text{C}$, the color is gray to yellowish-gray and the laser light may reach deep in the sample. The spatial distribution of the particle size, therefore, is less important for those fibers.

Figure 8 plots the values of L_{EM} and L_{111} as a function of $2r_s$ as deduced by the curve fit to the Raman spectra. The difference between L_{111} and L_{EM} indicates that each particle consists of a number of crystallites. The $2r_s$ is correlated with L_{EM} but not with L_{111} —namely, the particle size rather than the crystallite size characterizes the polariton state in small particles. The value of L_{EM} is larger by a factor of about 5 than $2r_s$ as shown by the straight line in Fig. 8. The curve fit to the Raman spectrum of small GaP particles also gives a particle size smaller than L_{EM} by a factor of 4.5.³⁶ The discrepancy in the particle size comes, in part, from underestimation of the particle size in the curve-fitting process for the Raman spectrum as explained in Sec. II B; i.e., neglect of the angular dependence of the scattering efficiency. The disagreement is quite large (a factor of 10–100) for sample no. 2 as shown in Table I. The MG formula is not valid for this size of particle.

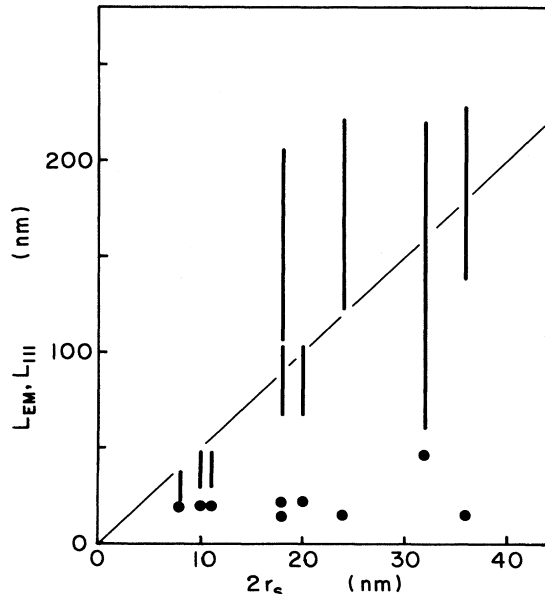


FIG. 8. Particle size (L_{EM}) and size of crystallite (L_{111}) plotted as a function of $2r_s$ estimated from the curve fit to the Raman data. Vertical bars indicate the distribution of L_{EM} and solid circles show L_{111} . The straight line presents $L_{EM} = 10r_s$.

V. DISCUSSION

A. Effects of grain boundary on phonon states

We have obtained a reasonably good fit to the experimental spectra with the MG and/or Mie's formula if the particle size is larger than about 30 nm and smaller than 200 nm. The MG approach for isotropic materials predicts that the case of $f=1$ is identical to the bulk crystal. In this model, a particle consisting of many crystallites by coalescence is treated as a large crystal with the size equal to the particle. This prediction agrees with the experimental observation that the particle size estimated from the Raman data shows a good correlation with L_{EM} rather than L_{111} as shown in Fig. 8. This model is equivalent to neglect of any surface mode at the interface between crystallites. The polariton can propagate through the grain boundary even with a misorientation because it has an electromagnetic component. We may expect, however, an increase of the damping in its phonon component caused by the interface between the crystallites.

The width of the absorption peak decreases in the sample containing hydrogen [Fig. 5(a)] compared to that without it [Fig. 5(b)]. The crystallite size is expected to be smaller in the former than in the latter. Thus the difference in the linewidth may come from the termination of the dangling bond for the atoms at the crystallite surface by hydrogen.

B. Effects of surface on the frequency and damping of the TO phonon

The damping both in the core (Γ_c) and in the shell (Γ_s) increases, especially Γ_s , with a decrease in r_s . ω_T decreases at the same time. Although there is scatter of the data for ω_T [Fig. 7(a)] and the damping [Fig. 7(c)], we find good correlation between ω_T and the damping as plotted in Fig. 9(a). This correlation may suggest that both the decrease in ω_T and the increase in the damping are caused by extra anharmonicity at the surface. The scatter of data in Figs. 7(a) and 7(c) suggests that the extra anharmonicity is characterized not only by the particle size but also by other factors, such as defects at the interface between the crystallites, geometrical shape of the particle, or scheme of the atomic bonding between the surface atom and the atom(s) in the surrounding medium.

Anharmonicity of the optical phonon in the bulk SiC crystal comes from a decay of the phonon into two LA phonons, where the damping of the TO phonon is approximated at a temperature T by

$$\Gamma(T) = \Gamma_0 + \Gamma_a(n_q(\omega_T/2, T) + \frac{1}{2}), \quad (23)$$

with $\Gamma_0 = 0$ and $\Gamma_a = 4 \text{ cm}^{-1}$.³⁵ Our preliminary result of the temperature dependence of the Raman spectrum fits Eq. (23) using $\Gamma_a = 4 \text{ cm}^{-1}$ and $\Gamma_0 = 2.6 \text{ cm}^{-1}$ for sample no. 1. Furthermore, the temperature coefficient of ω_T coincides with that of the 3C-SiC crystal.³⁵ These results indicate that the extra damping in the small particle comes from an increase in the temperature-independent term Γ_0 , i.e., the lattice imperfection near the surface

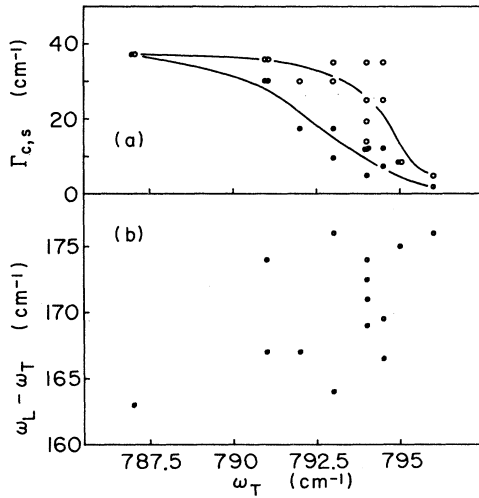


FIG. 9. (a) Phonon dampings plotted as a function of ω_T deduced from the Raman data. Solid circles and open circles denote Γ_c and Γ_s , respectively. (b) The LT splitting plotted with respect to ω_T .

does not contribute to the extra damping through enhancement of the anharmonicity up to several hundred K, but it contributes to an increase in the elastic-scattering rate of the TO phonon. Another role of the lattice imperfection near the surface is to soften the TO phonon in small particles.

The particle-size dependence of the absorption spectra given in Sec. IV A is explained if we introduce a "surface layer" which exhibits an amorphouslike absorption spectrum. Its thickness is estimated to be slightly less than 1 nm because the particle of $L_{EM} \approx L_{111} \approx 2$ nm shows mostly the amorphouslike absorption spectrum with superposition of the weak crystal-like spectrum [Fig. 5(c)]. Although the surface phonon (not the surface polariton) may contribute to the deformation of the absorption and Raman spectra of small particles, the width of the amorphouslike absorption line ($200\text{--}300 \text{ cm}^{-1}$) is too large to attribute the enhanced linewidth to the surface phonon. Here the surface phonon is located just below or resonating with the bulk-phonon band.³⁷ Thus the imperfection of the atomic arrangement in the surface layer causes the broad amorphouslike absorption line. This imperfection also contributes to the extra-anharmonicity of the TO and LO phonons inside the particle.

This model with the surface layer suggests that the volume which gives rise to the crystal-like spectrum is comparable to that of the surface layer for a particle size of about 10 nm. This value agrees with the critical size for the transformation of the Raman spectrum from crystal-like to amorphouslike.¹³⁻¹⁵ The surface layer is much thinner than the shell without a free carrier (5-40 nm thick), i.e., a surface layer exists at the surface of the shell.

C. Quenching of the LT splitting

The LT splitting decreases for smaller particles as shown in Fig. 7. A decrease in the LT splitting is ob-

served also in GaP ion-implanted with Ar^+ .³⁸ The splitting becomes smaller at higher doses. The decrease has been attributed to the disruption of ionic ordering by implantation damage, which weakens the Coulombic interaction responsible for the LT splitting. In the present case, the finite particle size causes a decrease in the splitting. In the following, the size dependence of the LT splitting is explained in terms of decrease in the polarization: The polarization may be expressed by

$$P = Ne^*U, \quad (24)$$

where N is the number of atoms in a unit volume, e^* the effective charge, and U the relative displacement of the anion and cation. The macroscopic electric field decreases in the small particles due to an absence of the contribution from the hypothetical atoms outside the particle. This effect is approximated by assuming a surface layer with no contribution to the polarization. Furthermore, the atoms located at the surface of the particle may not contribute to the polarization because there is no counterion outside the particle. If there is disorder in the atomic arrangement for the surface layer, the contribution from this layer to the polarization may be smaller than expected for a layer with the perfect atomic arrangement. Taking into account these effects, Eq. (24) is replaced for a sphere with a radius of r_s by

$$P = Ne'^*U, \quad (25)$$

where

$$e'^* = e^*(r_s^3 - a_s r_s^2) / r_s^3, \quad (26)$$

where a_s is the effective thickness of the layer without a contribution to the polarization. Since the mechanical coupling between the ions is a rather short-range force, the effect of the surface atoms exists only in a few atomic layers from the surface. Thus the size dependence of ω_T is much weaker than that of ω_L . Finally, ω_L is obtained from

$$\omega_L^2 - \omega_T^2 = 4\pi N(e'^*)^2 / M\epsilon_\infty, \quad (27)$$

where M is the reduced mass of the ions. Here, ϵ_∞ is considered to be unchanged because only the electronic polarization contributes to ϵ_∞ and the number of electrons is the same for atoms at the surface and inside the particle. This model predicts a monotonic decrease in the LT splitting for smaller particles. The approximation given above is not valid in particles smaller than a few nanometers, where the number of the surface atoms are comparable to, or larger than, that of atoms inside the particle. Vibrational states of those particles may not be expressed by the concept of the phonon. There is no concept of the TO or LO phonon for clusters consisting of a few atoms.

The dashed-dotted line in Fig. 7(b) indicates the LT splitting calculated from Eq. (27) with $a_s = 0.13$ nm. Since the actual particle size is larger by a factor of about 5 than $2r_s$, the real value of a_s is expected to be around 0.65 nm. This value is larger than the nearest Si-C distance of 0.19 nm and smaller than the thickness of the surface layer of ≈ 1 nm. Although there are uncertain-

ties in this mode (e.g., effect of the impurity, nature of the disordered surface layer), we find a good agreement between the experimental result and the calculated curve for $2r_s < 20$ nm, or $L_{EM} < 100$ nm. The disagreement for larger particles seems to be a consequence of the retardation effect, which becomes important for particles larger than $\lambda/2n \approx 100$ nm—namely, the Raman line due to the bulk TO phonon is located at a lower frequency than real ω_T because of the retardation effect. Here λ is the wavelength of the laser light and n the refractive index of the particle. If we take into account the retardation in the estimation of ω_T , the ω_T 's are expected to be higher than those in Fig. 7(a) and the $(\omega_L - \omega_T)$'s to be lower than those in Fig. 7(b) by a couple of wave numbers for $2r_s > 20$ nm.

D. Validity of the phonon-coefficient model

Size dependence of the phonon frequencies and the damping might be explained in terms of the uncertainty in the phonon wave vector; i.e., "spatial correlation" model.^{39,40} This model has been successful in explaining the Raman spectra of mixed crystals and those of implantation-damaged crystals. The model predicts, however, much smaller particle size than our observation of L_{EM} and L_{111} , or otherwise much smaller frequency shift for a given particle size. Furthermore, the predicted increase in the width of the Raman line is much smaller than the experimental result. For example, the expected frequency shifts for sample no. 4 are 0.5 cm^{-1} (ω_T) and 1.5 cm^{-1} (ω_L) with the use of a correlation length equal to $L_{111} = 19$ nm ($< L_{EM}$), while they are 4 and 14 cm^{-1} , respectively, in our experiment. In the calculation we use the phonon-dispersion curve obtained for the [111] direction.⁴¹ The spatial correlation model, therefore, fails in quantitative explanation of the particle-size dependence of the phonon states. Difficulty in the application of the spatial correlation model comes from existence of the surface layer which causes the extra-anharmonicity, as dis-

cussed in Sec. V B. The shift of ω_T and ω_L might be interpreted in terms of stress (tension) in the particles. This is, however, not the case, because the difference in the particle-size dependences of ω_T and ω_L as shown in Figs. 7(a) and 7(b) is much larger than the difference in the pressure coefficients, $\partial\omega_T/\partial P$ and $\partial\omega_L/\partial P$, of 20%.⁴²

VI. CONCLUSIONS

The infrared and Raman spectra of small SiC particles agree with the calculated curves with the MG and/or Mie's formula using parameters slightly different from those for the bulk crystal. Those spectra are characterized by the particle size rather than the size of crystallites constituting the particle. The TO-phonon frequency decreases and its damping increases with decrease in the particle size caused by the elastic scattering of the TO phonon due to the imperfections in the atomic arrangement in the surface layer. The LT splitting also diminishes with decrease in the particle size due to an absence of the macroscopic electric field by the hypothetical atoms outside the particle and to the quenching of the polarization by the atoms near the surface of the particle. The crystal-like spectrum is superposed on the amorphouslike spectrum for particles larger than a couple of nanometers and smaller than a few tens of nanometers. The surface layer with its thickness of about 1 nm contributes to the amorphouslike spectrum.

ACKNOWLEDGMENTS

The authors would like to thank Professor C. Horie for valuable discussion and F. Chida for assistance in the infrared measurement. They appreciate Dr. S. Yamada of Toyota Central R&D Labs, Inc. for providing a ceramic mortar. Thanks are also due to Dr. S. Ichikawa and S. Mitsuno of Nippon Carbon for providing some of the SiC fibers measured in this work.

*Present address: Department of Basic Science, Ishinomaki Senshu University, Ishinomaki, Miyagi 986, Japan.

†Present address: Central Research Laboratory, Ube Industries Ltd., Ube, Yamaguchi 755, Japan.

‡Present address: Department of Metallurgical Engineering, College of Engineering, University of Osaka Prefecture, Sakai, Osaka 591, Japan.

¹A. I. Ekimov, A. L. Efros, and A. A. Onushchenko, *Solid State Commun.* **56**, 921 (1985).

²J. Warnock and D. D. Awschalom, *Appl. Phys. Lett.* **48**, 425 (1986).

³C. J. Sandroff, D. M. Hwang, and W. M. Chung, *Phys. Rev. B* **8**, 5953 (1986).

⁴R. Ruppini and R. Engelman, *Rep. Prog. Phys.* **33**, 149 (1970).

⁵L. Genzel and T. P. Martin, *Surf. Sci.* **34**, 33 (1973).

⁶R. Ruppini, *J. Phys. C* **8**, 1969 (1975).

⁷M. Takagi, *J. Phys. Soc. Jpn.* **9**, 359 (1954).

⁸Ph. Buffat and J.-P. Borel, *Phys. Rev. A* **13**, 2287 (1976).

⁹T. Matsubara, Y. Iwase, and A. Momokita, *Prog. Theor. Phys.* **58**, 1102 (1977).

¹⁰Y. Kashiwase, I. Nishida, Y. Kainuma, and K. Kimoto, *J. Phys.* **38**, C2-157 (1977).

¹¹J. Harada and K. Ohshima, *Surf. Sci.* **106**, 51 (1981).

¹²Z. Iqbal, S. Veprek, A. P. Webb, and P. Capezzuto, *Solid State Commun.* **37**, 993 (1981).

¹³S. Hayashi, M. Ito, and H. Kanamori, *Solid State Commun.* **44**, 75 (1982).

¹⁴S. Hayashi and H. Abe, *Jpn. J. Appl. Phys.* **23**, L824 (1984).

¹⁵T. Okada, T. Iwaki, K. Yamamoto, H. Kasahara, and K. Abe, *Solid State Commun.* **49**, 809 (1984).

¹⁶C. J. Sandroff and L. A. Farrow, *Chem. Phys. Lett.* **130**, 458 (1986).

¹⁷Y. Sasaki, Y. Nishina, M. Sato, and K. Okamura, *Yogyo-Kyokai-Shi* **94**, 897 (1986).

¹⁸J. C. Maxwell-Garnet, *Philos. Trans. R. Soc. London Ser. A* **203**, 385 (1904).

- ¹⁹G. Mie, *Ann. Phys. (Leipzig)* **25**, 377 (1908).
- ²⁰Y. Sasaki, Y. Nishina, M. Sato, and K. Okamura, in *Proceedings of the Nineteenth International Conference on the Physics of Semiconductors, Warsaw, 1988*, edited by W. Zawadski (Institute of Physics Polish Academy of Sciences, Warsaw, Poland, 1988), p. 823.
- ²¹K. Yamamoto, K. Kimura, M. Ueda, H. Kasahara, and T. Okada, *J. Phys. C* **18**, 2361 (1985).
- ²²R. Ruppin, *Surf. Sci.* **51**, 140 (1975).
- ²³T. P. Martin and L. Genzel, *Phys. Rev. B* **8**, 1630 (1973).
- ²⁴D. T. Hon and W. L. Faust, *Appl. Phys.* **1**, 241 (1973).
- ²⁵G. Irmer, V. V. Toporov, B. H. Bairamov, and J. Monecke, *Phys. Status Solidi B* **119**, 595 (1983).
- ²⁶H. Yugami, S. Nakashima, A. Mitsuishi, A. Uemoto, M. Shigeta, K. Furukawa, A. Suzuki, and S. Nakajima, *J. Appl. Phys.* **61**, 354 (1987).
- ²⁷M. V. Klein, B. N. Ganguly, and P. J. Colwell, *Phys. Rev. B* **6**, 2380 (1972).
- ²⁸S. Ushioda and R. Loudon, in *Modern Problems in Condensed Matter Sciences Vol. 1, Surface Polaritons*, edited by V. M. Agranovich and D. L. Mills (North-Holland, Amsterdam, 1982), p. 535.
- ²⁹S. Yajima, *Philos. Trans. R. Soc. London Ser. A* **294**, 419 (1980).
- ³⁰Y. Sasaki, Y. Nishina, M. Sato, and K. Okamura, *J. Mater. Sci.* **22**, 443 (1987).
- ³¹U. Kreibitz, *Z. Phys. D* **3**, 239 (1986).
- ³²K. H. Rieder, M. Ishigame, and L. Genzel, *Phys. Rev. B* **6**, 3804 (1972).
- ³³Y. Hasegawa and K. Okamura, *J. Mater. Sci.* **18**, 3633 (1983).
- ³⁴K. Kunc, M. Balkanski, and A. Nusimovici, *Phys. Status Solidi B* **72**, 229 (1975).
- ³⁵D. Olego and M. Cardona, *Phys. Rev. B* **25**, 3889 (1982).
- ³⁶S. Hayashi and R. Ruppin, *J. Phys. C* **18**, 2583 (1985).
- ³⁷R. E. Allen, G. P. Alldredge, and F. W. de Wette, *Phys. Rev. B* **4**, 1161 (1971).
- ³⁸D. R. Myers, P. L. Gourley, and P. S. Peercy, *J. Appl. Phys.* **54**, 5032 (1983).
- ³⁹K. K. Tiong, P. M. Amiratharaj, F. H. Pollak, and D. E. Aspnes, *Appl. Phys. Lett.* **44**, 122 (1984).
- ⁴⁰P. Parayanthal and F. H. Pollak, *Phys. Rev. Lett.* **52**, 1822 (1984).
- ⁴¹D. W. Feldman, J. H. Parker, Jr., W. J. Choyke, and L. Patrick, *Phys. Rev.* **173**, 787 (1968).
- ⁴²D. Olego and M. Cardona, *Phys. Rev. B* **25**, 1151 (1982).